Journal of the Optical Society of Korea
Vol. 20, No. 1, February 2016, pp. 94-100

ISSN: 1226-4776(Print) / ISSN: 2093-6885(Online)
DOI: http://dx.doi.org/10.3807/JOSK.2016.20.1.094

A Coaxial and Off-axial Integrated Three-mirror Optical System with High Resolution and Large Field of View

Zhe Chen[1,2]*, Junqing Zhu[1,2], Jiantao Peng[1,2], Xingxiang Zhang[1], and Jianyue Ren[1]

[1]*Changchun Institute of Optics and Fine Mechanics and Physics, Chinese Academy of Sciences, Changchun, Jilin 130033, China*
[2]*University of Chinese Academy of Sciences, Beijing 10049, China*

(Received August 28, 2015 : revised January 8, 2016 : accepted February 1, 2016)

A novel optical design for high resolution, large field of view (FOV) and multispectral remote sensing is presented. An f/7.3 Korsch and two f/17.9 Cook three-mirror optical systems are integrated by sharing the primary and secondary mirrors, bias of the FOV, decentering of the apertures and reasonable structure arrangement. The aperture stop of the Korsch system is located on the primary mirror, while those of the Cook systems are on the exit pupils. High resolution image with spectral coverage from visible to near-infrared (NIR) can be acquired through the Korsch system with a focal length of 14 m, while wide-field imaging is accomplished by the two Cook systems whose focal lengths are both 13.24 m. The full FOV is 4°×0.13°, a coverage width of 34.9 km at the altitude of 500 km can then be acquired by push-broom imaging. To facilitate controlling the stray light, the intermediate images and the real exit pupils are spatially available. After optimization, a near diffraction-limited performance and a compact optical package are achieved. The sharing of the on-axis primary and secondary mirrors reduces the cost of fabrication, test, and manufacture effectively. Besides, the two tertiary mirrors of the Cook systems possess the same parameters, further cutting down the cost.

Keywords : Three-mirror system, Telescopes, Optical system design, On-axis, Off-axis
OCIS codes : (110.6770) Telescopes; (120.4570) Optical design of instruments; (220.4830) Systems design; (350.6090) Space optics

I. INTRODUCTION

Optical systems characterized by large apertures, long focal lengths and large fields of view (FOVs) are required by the application of high resolution, large spatial and spectral coverage space-to-earth observation. Compared with refractive optical systems, mirror systems are widely utilized in space-borne remote sensing, because of the absence of chromatic aberration, easiness of lightweight design [1], and the compact configuration.

Three-mirror systems are commonly adopted by remote sensors for the advantages of more freedoms in optimization, higher image quality and larger flat focal plane etc. over two-mirror systems. There are mainly three principal categories of three-mirror systems for various applications: the Wetherell type [2, 3] [Fig. 1(a)], the Korsch type [4, 5] (Fig. 1(b)) and the Cook type [6] [Fig. 1(c)]. With an axial pupil which is usually the secondary mirror and an off-axis FOV induced to eliminate the central obstruction, the Wetherell type has the virtues of large FOV, high optical performance, and it easily retains a telecentric final image. However, the absence of the intermediate image and the real exit pupil makes it difficult to control the stray light. Besides, the long distance between the primary and the secondary and the off-axis elements leads to a relatively bulky volume and complicates the manufacture and alignment. The Korsch type features flat field, an advantage of telephoto allowing the system to be folded in a compact envelope [7], an intermediate image where a field mask can be placed to help control the stray light and a real exit pupil. If necessary, a Lyot stop can be set on the exit pupil together with a heat shield, then effective baffling against stray heat is achievable [7, 8]. Considered as the off-axis section of a large parent on-axis Korsch type which is illustrated in Fig. 1(c), the Cook

*Corresponding author: chenzheyiyezhiqiu@126.com
Color versions of one or more of the figures in this paper are available online.

type inherits the features above. Furthermore, due to the off-axis pupil to remove the obstruction, higher-quality image and larger FOV can be achieved by the Cook type than the Korsch one with the same aperture, at the cost of a less-efficient package, a more complex manufacturing and a more demanding alignment. This is because the mirrors are off-axis and the aspheric departure on Cook type is several times higher than that on Korsch type.

In order to perform the detailed and general reconnaissance simultaneously and reduce the cost, we integrate two Cook type optical systems with large f-numbers into a small f-number Korsch type system to synthesize the advantages of the two types. Each system delivers a near diffraction-limited performance. The whole design consists of a concave primary mirror, a convex secondary mirror, three concave tertiary mirrors and is accommodated within a compact package by using four folding flat mirrors. The primary mirror and the secondary mirror are shared by the Korsch type and Cook type optical systems, which means the Cook systems image through the sub-apertures of these two mirrors of the Korsch system. Therefore, in the following text, we call them mutual mirrors.

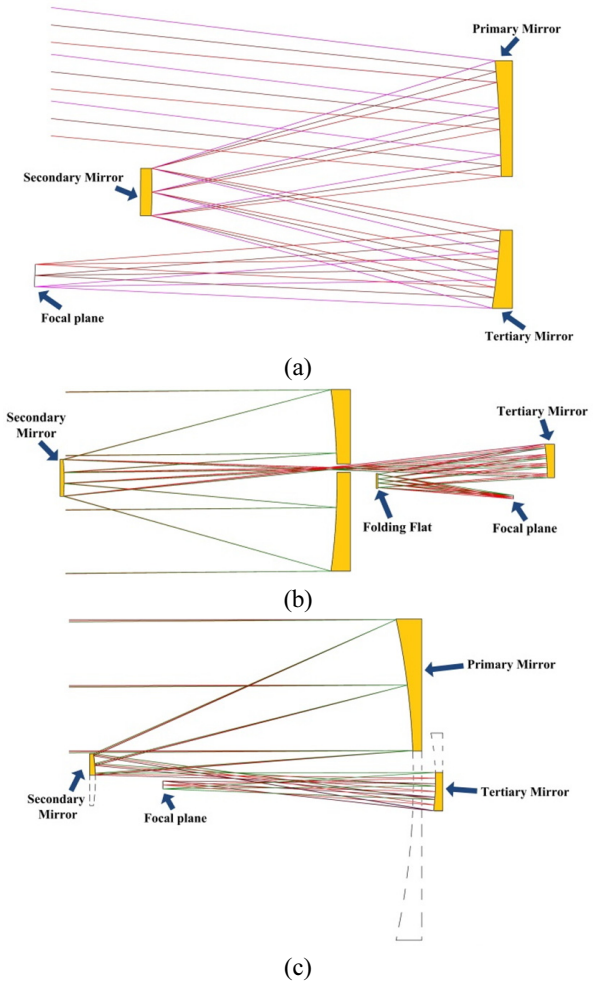

FIG. 1. Optics layouts of the three principal categories of three-mirror systems for various applications: (a) the Wetherell type; (b) the Korsch type; (c) the Cook system and its parent Korsch system.

II. DESIGN SPECIFICATION

Mathematical relationships between system parameters of remote sensing cameras can be expressed by Eqs. (1)~(3) [9].

$$f = Ha / d , \tag{1}$$

$$r = \frac{1.22\lambda}{D} f = 1.22\lambda F / \# \tag{2}$$

$$L = 2H \tan(\frac{FOV}{2}) \tag{3}$$

where f is the focal length, H is the altitude, a is the pixel pitch, d is the ground sampled distance (GSD) for a nadir viewing geometry, r is the radius of Airy disk, λ is the primary wave length of the working band, D is the entrance pupil diameter, $F/\#$ is the f-number, L is the cover width on the earth.

As is plotted in Fig. 2, the whole 4°×0.13° FOV includes three individual parts: the 1°×0.13° middle FOV, the 1.5°×0.13° right FOV and the 1.5°×0.13° left FOV, imaging through the Korsch system, the Cook system I and the Cook system II respectively. The left and right FOVs are symmetric about the Y axis. The FOV points marked in Fig. 2 are listed in Table 1. The design and optimization of the three individual systems are aiming at their own 0.13° wide FOVs. The technical specifications of the Korsch type and Cook type optical systems are listed in Table 2. Accordingly, the whole coverage width d = 8.7 + 13.1 + 13.1 = 34.9 km. The GSD of the middle 8.7 km coverage is 0.25 m in 0.38 ~ 0.78 μm band, and 0.46 m in 1.2 ~ 1.7 μm band respectively. The GSD of both the lateral 13.1 km coverage is 0.5 m in 0.38 ~ 0.78 μm band. The

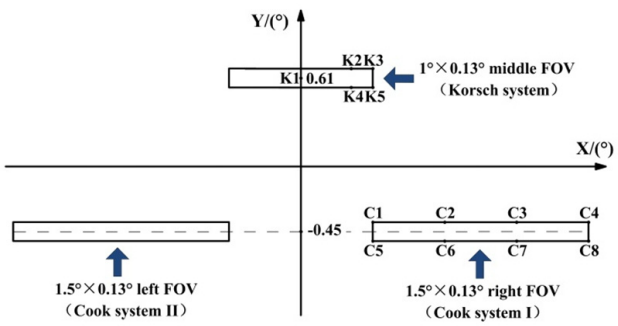

FIG. 2. The FOV distribution of the three sub-systems and the FOV points for image quality evaluation.

TABLE 1. Coordinates of FOV points marked on Fig. 2

FOV points	X/(°)	Y/(°)
K1	0	0.61
K2	0.35	0.675
K3	0.5	0.675
K4	0.35	0.545
K5	0.5	0.545
C1	0.5	-0.385
C2	1	-0.385
C3	1.5	-0.385
C4	2	-0.385
C5	0.5	-0.515
C6	1	-0.515
C7	1.5	-0.515
C8	2	-0.515

TABLE 2. The technical specifications of the Korsch type and Cook type optical systems

Parameters	Values		
System type	The Korsch system		The Cook system I/II
f-number	7.3		17.9
Focal length/m	14		13.24
Aperture/m	1.92		0.74
Field of view/°	1×0.13		1.5×0.13
Coverage width/km	8.7		13.1
Spectral bands/μm	0.38~0.78	1.2~1.7	0.38~0.78
Pixel size/μm	7	13	14
GSD/m	0.25	0.46	0.5

visible and NIR detectors can be mounted in parallel on the focal plane of the Korsch system for push-broom imaging.

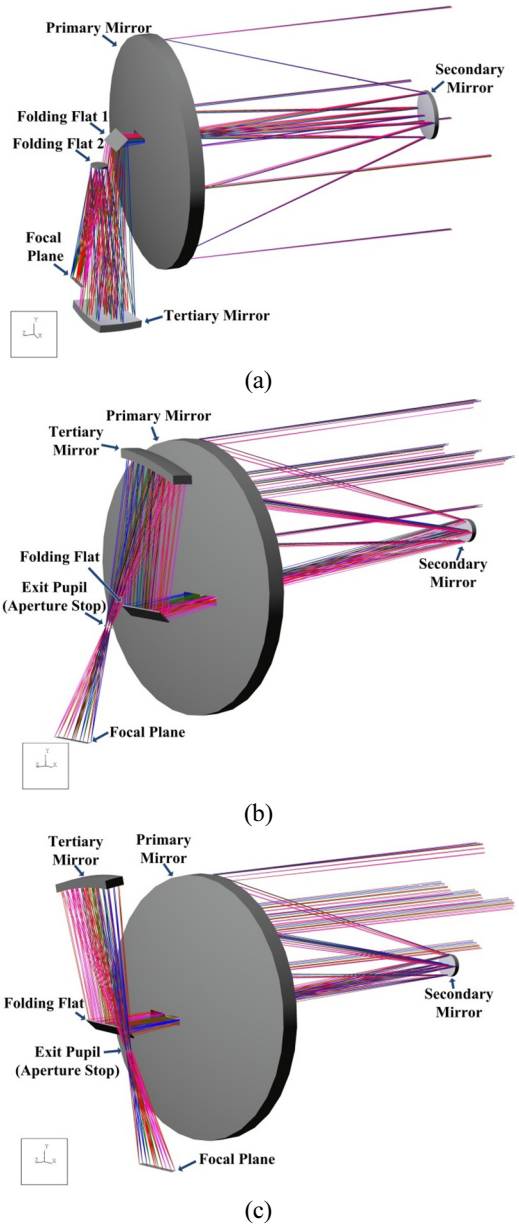

FIG. 3. Optical configurations: (a) the Korsch system, (b) the Cook system I, (c) the Cook system II.

III. OPTICAL SYSTEM DESIGN

The initial structure of the three-mirror optical system is attained by the mathematical derivation which has been presented in a variety of contexts [10-12]. Here, we focus on the optimization procedure of the integrated system.

The primary mirror is selected as the aperture stop of the Korsch system, while the aperture stops of the Cook systems are located at the exit pupils. According to Fig. 2 and Table 1, off-axis FOV of 0.61° along the Y axis is induced into the on-axis Korsch system to avoid the second obstruction caused by the focal plane. The off-axis FOVs along the Y axis of the two off-axis Cook systems are both -0.45°. These biases of FOVs, together with the packaging constraints, prevent the components from vignetting the beam and keep the intermediate images and the real exit pupils of different systems available.

The primary mirror and secondary mirror are conics. The three tertiary mirrors are aspheres with 6th order coefficient. The asphere surface sag is as follows:

$$z = \frac{ch^2}{1+\sqrt{1-(1+k)c^2h^2}} + \sum_{i=2}^{8} \alpha_i h^{2i} \tag{4}$$

Where c is the curvature at the pole of the surface, h is the radial distance with respect to the Z axis, k is the conic coefficient, α_i are the deformation coefficients. The Cartesian coordinates are shown in Fig. 3.

The optical axis, namely the common axis of the primary and secondary mirrors are parallel to the Z axis. Since the primary mirror and secondary mirror are mutual, during optimization, special attention is needed to limit the apertures of these two mirrors in Cook systems inside the effective apertures of the corresponding mirrors in the Korsch system. The parameters of the primary mirrors in different systems must be kept the same as they are varying, and so is the secondary mirror.

Driven by the character of the FOV, the two Cook systems are almost symmetric about the Y-Z plane, except for the tilts of the folding flats which are set differently deliberately to spatially separate the exit pupils. In other words, the location and the orientation of the two tertiary mirrors of the Cook systems are symmetric about the Y-Z plane when the folding mirrors are removed. Therefore, only one Cook system needs to be optimized, and then the parameters of the other one are set according to the result. The tilts and decenters of the tertiary mirrors in the Cook system are set as variables to further balance the aberrations of the off-axis FOVs, except for the curvatures, conic constants, aspheric coefficients and spaces.

Other considerations should be taken into account to (1) control the distance between the primary and the secondary mirrors; (2) restrict the obstruction area of the secondary mirror; (3) make allowance for the mechanical structures such as the stops and baffles.

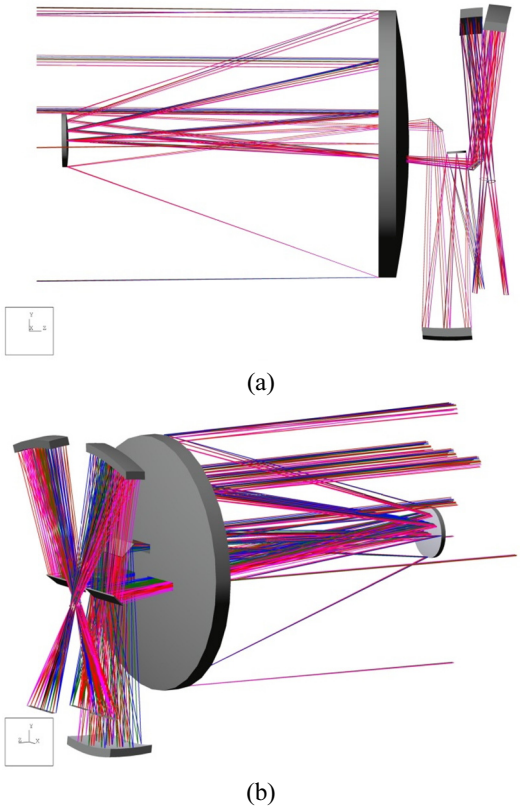

(a)

(b)

FIG. 4. Optical configurations of the whole system: (a) two-dimensional diagram, (b) three-dimensional diagram.

IV. CONFIGURATION OF OPTICAL SYSTEM

The optical configurations of the Korsch system, the Cook system I, the Cook system II are demonstrated in Fig. 3 (a), (b) and (c). And the whole system is illustrated in Fig. 4 (a) and (b). Table 3 lists the parameters of the powered surface after optimization. Table 4 lists the locations of the optical components, namely the local surface coordinates with respect to the vertex point of the primary mirror. The reference point of every mirror is its own vertex point.

Suppose the folding mirrors are removed and the position and the orientation of the tertiary mirrors are adjusted accordingly. Then, their decenters and tilts are listed in Table 5. Obviously, tertiary mirror of the Korsch system is on the common axis of the primary and secondary, while the tertiary mirrors of the two Cook systems are not, but are symmetric about the Y-Z plane.

The ray footprints of the mutual primary mirror are presented in Fig. 5. It's obvious that the footprints of the two Cook systems are within the envelope of the Korsch system and the primary mirror is axisymmetric, which reduces the difficulty of fabrication and test significantly compared to the off-axis equivalent. Here, we ignore the influence of the obstruction which will be discussed in the next chapter.

It's spatially adequate to install the field stops and the Lyot stops at the intermediate images and the real exit pupils respectively for stray radiation control. Together with

TABLE 3. Parameters of the powered surfaces

	Radius/mm	Conic	6^{th} order coefficient
Primary	-5777.652	-0.946	-
Secondary	-1523.678	-2.220	-
Tertiary (Korsch)	-2044.277	-0.448	-1.645×10^{-20}
Tertiary (Cook)	-1866.114	-0.454	-5.810×10^{-20}

the main baffle, the secondary mirror baffle, the primary central baffles and light shields, the stray light can be mitigated effectively. The folding flat 2 (Fig. 3 (a)) is located at the exit pupil of the Korsch system. There are enough room behind it for other subsystems to further improve the performance functionally if appropriate adjustments are made: (1) modify the folding flat 2 into a deformable mirror to compensate for the figure error of the primary and the system wavefront error [13, 14], (2) replace the flat mirror with a splitter and design a lens working in a different waveband to match the pupil and to widen the spectral range of the system. A compact package of *f*/5.0 ~ *f*/4.9 long and *f*/6.1 ~ *f*/5.8 high is achieved.

With almost the same size of a traditional Korsch system, the integrated system described above can accomplish high resolution and wide field (about 4 times of the traditional

TABLE 4. Locations of the optical components

	X location/mm	Y location/mm	Z location/mm	Pitch/°	Yaw/°
Primary	0	0	0	0	0
Secondary	0	0	-2317.734	0	0
Folding flat 1 (Korsch)	0	0	481.231	47.872	0
Tertiary (Korsch)	0	-1339.727	615.982	95.744	0
Folding flat 2 (Korsch)	0	-66.856	487.956	93.744	0
Focal plane (Korsch)	0	-1047.436	586.583	91.693	0
Folding flat (Cook I)	0	0	790.646	-46.000	0
Tertiary (Cook I)	11.690	918.586	814.613	-92.018	-0.019
Stop (Cook I)	11.166	-270.307	733.841	-82.583	18.761
Focal plane (Cook I)	12.347	-1082.921	744.095	-91.926	0.164
Folding flat (CookII)	0	0	790.646	-52.000	0
Tertiary (Cook II)	-11.690	893.530	1005.074	-104.018	0.019
Stop (Cook II)	-11.166	-252.590	678.882	-94.583	-18.761
Focal plane (Cook II)	-12.347	-1049.578	519.961	-103.926	-0.164

TABLE 5. Decenters and tilts of tertiary mirrors after removing the folding mirrors and adjusting the positions and the orientations accordingly

	Decenter X/mm	Decenter Y/mm	Tilt about X axis/°	Tilt about Y axis/°
Tertiary (Korsch)	0	0	0	0
Tertiary (Cook I)	11.690	-8.106	-0.178	-0.0188
Tertiary (Cook II)	-11.690	-8.106	-0.178	0.0188

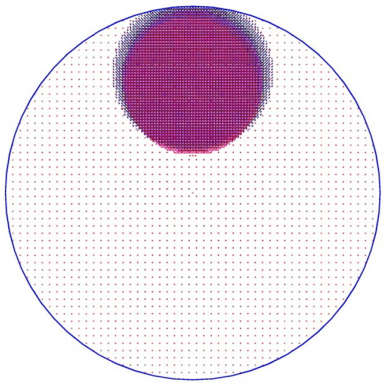

FIG. 5. Ray footprints of the mutual primary mirror.

one) remote sensing simultaneously, only at the cost of two more tertiary mirrors. The parameters of the two tertiary mirrors in the Cook systems are identical to each other. Besides, the primary and secondary mirrors of the on-axis Korsch system are shared with the Cook systems. Therefore, compared to three individual three-mirror optical systems, the fabrication and test are simplified dramatically. And the symmetry of the on-axis optical elements makes the system less sensitive to misalignments.

V. OPTICAL PERFORMANCE

Since the FOV is symmetric about the Y-Z plane, as illustrated in Fig. 2 and Table 1, five and eight representative field points of the Korsch system and Cook system are selected respectively to evaluate the image quality.

When the pupil is obscured, the shape and size of the diffraction-limited point spread function (PSF) are influenced by the obscuration ratio. If the obstruction is centrally symmetric, the increase of the obscuration ratio leads to the reduction of the first maximum and the enhancement of the second maximum, thus decreases and reshapes the Modulation Transfer Function (MTF) curves [15]. Here, we ignore the effect of the secondary baffle, as is shown in Fig. 6. the obstruction of the Korsch system caused by the spiders and the secondary mirror is not circular symmetry. The shape of PSF and the MTF in different directions will change correspondingly. The quality evaluation is performed taking into account the obstruction. The Cook systems are unobscured according to Fig. 4(a).

The spot diagram of the Korsch system is shown in Fig. 7. According to Eq. (2), the radiuses of Airy disks in visible (black circle) and NIR (red circle) spectrum ranges are 5.16 μm and 12.9 μm. Fig. 8 illustrates the spot diagram of the

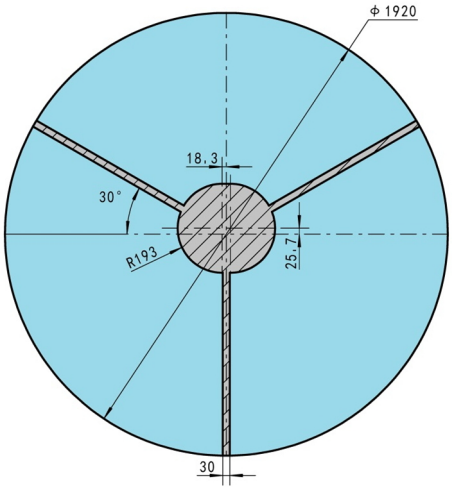

FIG. 6. Obstruction of the Korsch system.

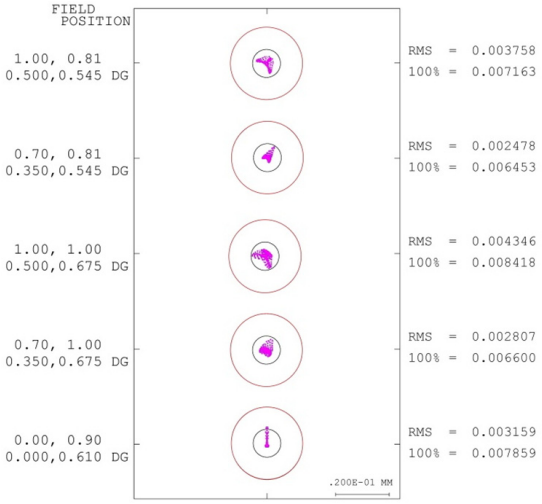

FIG. 7. Spot diagram of the Korsch system.

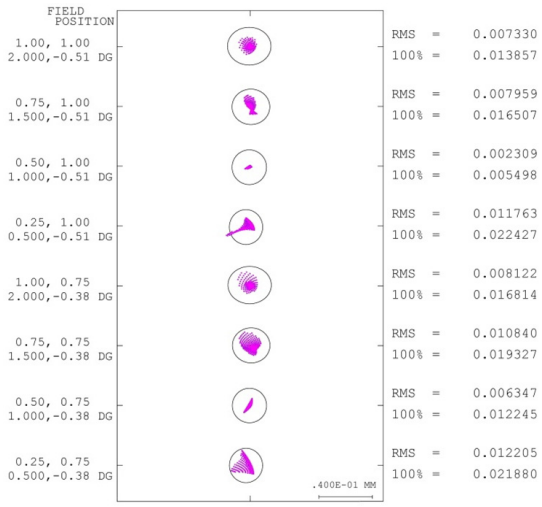

FIG. 8. Spot diagram of the Cook system.

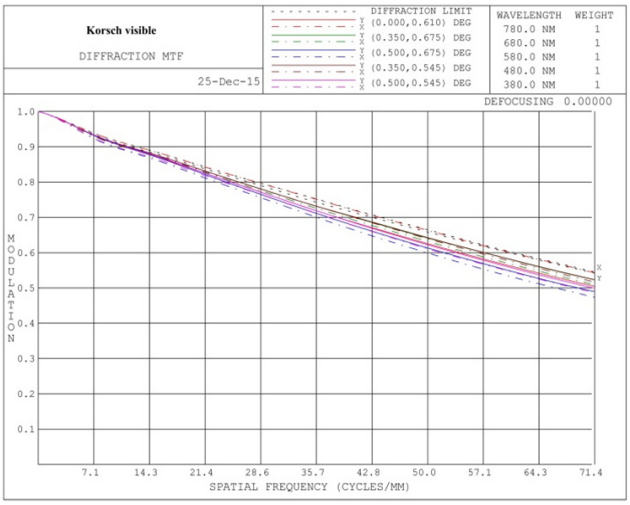

(a)

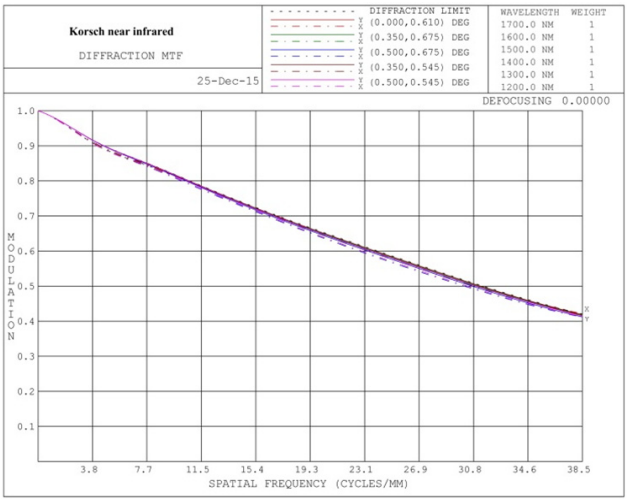

(b)

FIG. 9. MTF curves of the Korsch system: (a) the visible range, (b) the NIR band.

Cook system, and the radius of the Airy disk in visible band is 12.7 μm. The root mean square (rms) spot diameters all over the field are less than the Airy disks in different bands, and are within two pixels.

The MTF curves for visible and NIR bands of Korsch system are shown in Fig. 9(a) and (b). Figs. 10(a) and (b) are for the Cook system. Over the respective FOVs, the MTF values of the Korsch system are above 0.474 and 0.412 in visible and NIR bands, and the MTF of the Cook system is above 0.392 at the corresponding Nyquist frequencies (71.4 lp/mm, 38.5 lp/mm and 35.7 lp/mm).

VI. CONCLUSION

We have presented the optical design which integrates an f/7.3 Korsch with two f/17.9 Cook systems. The system consists of a mutual concave primary mirror, a mutual convex

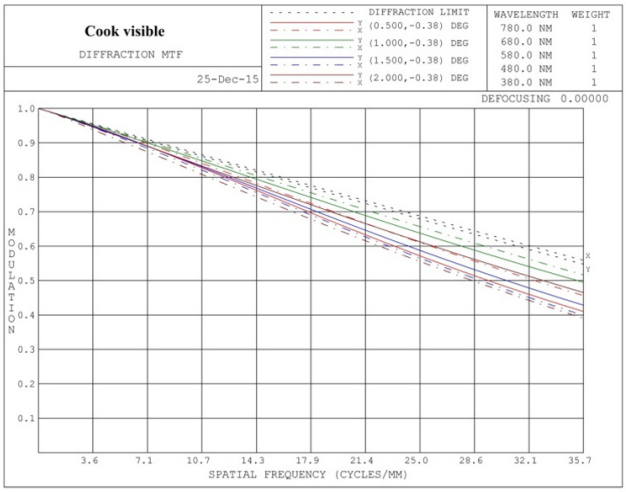

(a)

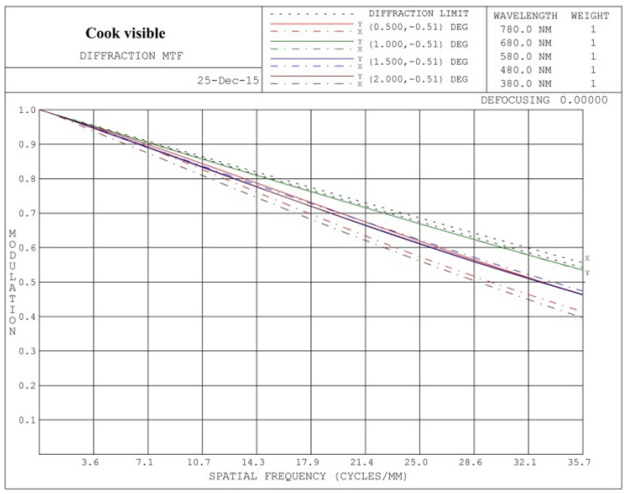

(b)

FIG. 10. MTF curves of the Cook system: (a) the FOV points of C1~C4, (b) the FOV points of C5~C8.

secondary mirror, three concave tertiary mirrors and four flat mirrors which fold the optical path into a compact envelope. The optimization strategy, feasibility of manufacture and alignment are analyzed. At the altitude of 500 km, the GSD of 0.25 m in visible range (0.38 ~ 0.78 μm) and 0.46 m in NIR band (1.2 ~ 1.7 μm) over a FOV of 1×0.13° can be attained through the Korsch system with a focal length of 14 m, the GSD of 0.5 m in visible range over two lateral FOVs of 1.5×0.13° can be attained through the two Cook systems whose focal lengths are both 13.24 m. The whole strip FOV is 4×0.13°, which covers an area of 34.9 km×1.1 km on the earth. The intermediate images and the real exit pupils in the whole system are all available for stray light suppressing. Near diffraction-limited image quality is achieved all over the FOV and the spectrum ranges. The ability of high resolution, large field of view and multi-spectral imaging make it a promising candidate for a remote sensing optical system.

ACKNOWLEDGMENT

This work is funded by the National High Technology Research and Development Program of China (863 Program) (No. 863-2-5-1-13B).

REFERENCES

1. H. Xu and Y. Guan, "Structural design of 1m diameter space mirror component of space camera," Optics and Precision Engineering **21**, 1488-1495 (2013).
2. W. Wetherell and D. Womble, "All-reflective three element objective," U.S. Patent 4240707 (1980).
3. D. Xue, "Integrated manufacturing technology of off-axis three-mirror anastigmatic system," Chin. Opt. Lett. **12(s2)**, S21202 (2014).
4. D. Korsch, "Astigmatic three-mirror telescope," Appl. Opt. **16**, 2074-2077 (1977).
5. D. Korsch, "Closed form solution for three-mirror telescopes, corrected for spherical aberration, coma, astigmatism, and field curvature," Appl. Opt. **11**, 2986-2987 (1972).
6. L. G. Cook, "Three-mirror anastigmat used off-axis in aperture and field," in *Proc. Huntsville Technical Symposium* (International Society for Optics and Photonics, USA, 1979), pp. 207-211.
7. M. L. Lampton, M. J. Sholl, and M. E. Levi, "Off-axis telescopes for dark energy investigations," Proc. SPIE **7731**, 77311G (2010).
8. X. L. Li, M. Xu, and Y. T. Pei, "Optical design of an off-axis five-mirror-anastigmatic telescope for near infrared remote sensing," J. Opt. Soc. Korea **16**, 343-348 (2012).
9. X. L. Li, M. Xu, X. D. Ren, and Y. T. Pei, "An optical design of off-axis four-mirror-anastigmatic telescope for remote sensing," J. Opt. Soc. Korea **16**, 243-246 (2012).
10. D. Korsch, "Design and optimization technique for three-mirror telescopes," Appl. Opt. **19**, 3640-3645 (1980).
11. J. H. Pan, *The Design, Manufacture and Test of the Aspheric Optical Surfaces* (Science Press, Beijing, China, 2004), Chapter 5.
12. J. U. Lee and S. M. Yu, "Analytic design procedure of three-mirror telescope corrected for spherical aberration, coma, astigmatism, and Petzval field curvature," J. Opt. Soc. Korea **13**, 184-192 (2009).
13. M. Laslandes, S. Pellegrino, J. Steeves, and K. Patterson, "Optimization of electrode configuration in surface-parallel actuated deformable mirrors," Proc. SPIE **9148**, 914843 (2014).
14. M. Laslandes, E. Hugot, M. Ferrari, C. Hourtoule, C. Singer, C. Devilliers, C. Lopez, and F. Chazallet, "Mirror actively deformed and regulated for applications in space: design and performance," Opt. Eng. **52**, 091803 (2013).
15. R. N. Wilson, *Reflecting Telescope Optics* (Springer, Berlin, German, 2004), Chapter 3.